



ERMESS: extreme wind risk assessment for building portfolios

Francesco Pandolfi¹ · Georgios Baltzopoulos¹ · Iunio Iervolino¹

Received: 26 August 2022 / Accepted: 24 November 2022 / Published online: 7 December 2022
© The Author(s), under exclusive licence to Springer Nature B.V. 2022, corrected publication 2022

Abstract

The increasing attention of stakeholders to extreme winds impacting the built environment is driving towards the adoption of probabilistic risk assessment methods, which aim at the stochastic modelling of three main risk components: hazard, vulnerability (or fragility), and exposure. Taking from seismic risk assessment, the hazard is typically expressed in terms of exceedance rate of an intensity measure of the natural event, usually related to wind speed, and the risk metric is the expected annual loss or the exceedance rate of the loss. On these premises the extreme wind risk assessment software, ERMESS, has been developed for risk assessment for portfolios of buildings. It integrates recent global- and regional-scale hazard maps for extreme wind events, that is, cyclones and tornadoes, and a database of more than five-thousand building- and component-level wind vulnerability and fragility functions from the literature. A procedure to develop building-level fragility models, based on existing component-level fragility functions, was also developed and embedded in ERMESS. Finally, the exposure (i.e. consequence) models are based on information provided by the insurance industry. The paper illustrates the software by means of proof-of-concept applications that show how ERMESS can be effective in wind risk assessment.

Keywords Performance-based wind engineering · Wind hazard · Wind fragility · Wind vulnerability · Computer-aided risk assessment

1 Introduction

According to the 2019 Global Natural Disaster Assessment Report (ADREM et al., 2020), out of 90.6 million people around the world impacted by major natural disasters that year, 34.5% were affected by storms, 32.7% by floods, 31.2% by droughts, and less than 2% by other types of events. In terms of direct economic losses worldwide, which amounted to \$121.856 billion, 47.53% was caused by storms. Of all climate-, weather-, and water-related disasters, one-third of human and economic losses are due to tropical cyclones. It has been estimated that each year sees the occurrence, on average, of 84

✉ Iunio Iervolino
iunio.iervolino@unina.it

¹ Dipartimento di Strutture per l'Ingegneria e l'Architettura, Università degli Studi di Napoli Federico II, Naples, Italy

such events that lead to 43 deaths and \$78 million in economic losses per day (WMO 2021). These data, together with the trend of exposure growth in extreme wind-prone areas, explain the rising attention of the international community on risk assessment and management of this kind of natural hazards (Ward et al. 2020).

Risk assessment can be seen as a probabilistic characterization of future losses that may be the result of natural (and/or other) hazards impacting the exposed assets. One of the risk management strategies is risk transfer, such as insurance, where the premium should be based on such an assessment. Risks due to certain natural hazards, such as earthquakes and wildfires, have a longer history of being studied than wind, which came to attention more recently. This may also be due to the fact that winds, with the exception of tornadoes, were considered less a life threat because of the possibility for prior warnings (van de Lindt and Dao 2009).

Engineering risk analysis is based on the decomposition in three probabilistic models: hazard, vulnerability (or fragility), and exposure. In the quantitative approach, hazard is typically represented by the rate with which an intensity measure of the phenomenon, for example, 3-s gust wind speed at an altitude of 10 m, is larger than a threshold, at the site of interest. Fragility [vulnerability] refers to the probability of the exposed asset to suffer damage [loss] exceeding a threshold, as a function of the intensity measure. Exposure models the value of the consequences of damage, for example, the conditional probability of exceeding some monetary loss, given the damage suffered by the asset. In this framework, the performance-based wind engineering (PBWE) method has been pioneered by Paulotto et al. (2004) that adapts the approach proposed for performance-based earthquake engineering (PBEE) (Cornell and Krawinkler 2000).

The scope of the study presented herein was to develop an application-ready wind risk assessment tool for building portfolios to be used in insurance applications, based on literature and industry models for hazard, fragility and/or vulnerability, and exposure. The result is ERMESS, a PBWE-based extreme wind risk assessment software, which is discussed in the following. ERMESS can be seen as a wind risk counterpart to similar tools developed for the seismic case, i.e. FRAME (Petruzzelli 2013; Petruzzelli and Iervolino 2014). In ERMESS, hazard is treated by considering two models corresponding to the most intense of all non-synoptic (Hangan and Kareem 2021) and synoptic wind events, which are, respectively, tornadoes and tropical cyclones. Regarding fragility, a database of fragility curves (building-, component-, and element-level) was built based on a specifically developed taxonomy, which leads ERMESS to contain more than five thousands vulnerability/fragility functions. Moreover, it features a procedure allowing to derive a building fragility function based on the fragility functions of the wind-vulnerable components present in the database. Exposure is represented in the software by means of direct loss models, which have been provided by the industry. Based on these components, ERMESS enables wind risk assessment in terms of expected annual loss, or the annual rate of a loss threshold exceedance. The assessment is building- and site-specific and exploits existing models; therefore, it does not require dedicated site-specific wind hazard assessment and/or building-specific analysis, at least in principle, and is thus suitable for medium-scale or portfolio (industrial) applications. Larger-scale applications are also possible, although the software is not optimized for multi-site input. Besides the collection of the embedded models, significant development effort in ERMESS was required to make them interoperable, for example rendering the intensity measures between hazard and fragility compatible, as well as the derivation of building-level fragility functions, based on a suitable taxonomy and available component fragilities.

The remainder of this paper is structured such that, after the introduction of the considered quantitative wind risk assessment framework, the hazard, fragility, and loss models are discussed. Regarding the hazard, the considered global- and regional-scale hazard maps and hazard curves are introduced, along with procedures for intensity measure conversion. Concerning the fragility/vulnerability models, the focus is on the discussion of the developed taxonomy and compiled database. Special attention is given to the fragility composition method, to obtain wind fragility from components’ fragility. After ERMESS and its graphical user interface (GUI) are introduced, illustrative applications show its capabilities. Some final remarks close the paper.

2 Wind risk assessment framework

Although the effects of extreme winds are addressed in building codes—e.g. the design of buildings in the USA subjected to hurricanes (ASCE 2022)—the difficulty in quantifying the economic losses associated with these phenomena remains (Lee and Rosowsky 2005). Various methodologies can be found in the literature for the evaluation of structural performance to wind, such as the analysis of loss data (Khanduri and Morrow 2003) and fault tree analysis (Unanwa et al. 2000), but the state of the art consists of developments within the PBWE framework (Ciampoli et al. 2011; Depina et al. 2021; Le and Caracoglia 2021; Ouyang and Spence 2019, 2020, 2021). PBWE, similar to PBEE, quantifies the risk of a structure to extreme wind through some metric that is sometimes termed as the *decision variable* (e.g. the economic loss resulting from windstorms). Such an assessment usually involves the definition of damage states, DS, that are proxy for the condition of the asset of interest from which some losses may be anticipated. According to PBEE, the risk of a structure is expressed as the rate of exceedance of a loss threshold, λ_l , by successive applications of the total probability theorem:

$$\lambda_l = \int_{IM} \sum_{j=1}^{n_{ds}} G_{L|DS, IM}(I|ds_j, im) \cdot P[DS = ds_j|im] \cdot |d\lambda_{im}| \tag{1}$$

In the equation, λ_{im} represents the so-called hazard curve (more discussion to follow), which is the plot of a function that provides the exceedance rate of an intensity measure IM (e.g. wind speed) of the phenomenon of interest (Fig. 1—left). Thus, the term

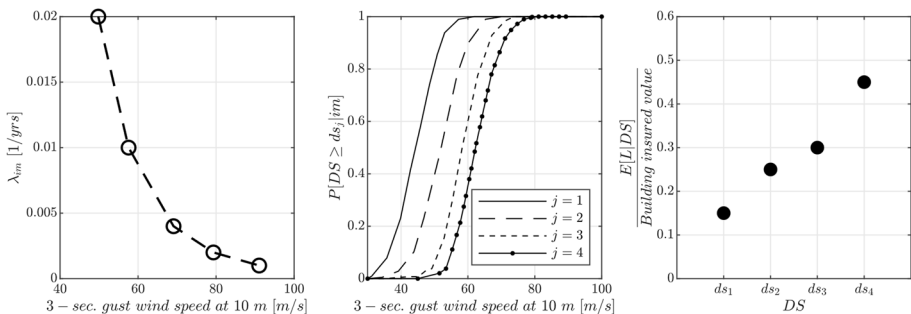


Fig. 1 Examples of risk components: Miami tropical cyclone hazard curve (CIMNE 2013), residential building fragility curves (FEMA 2005), and consequence function

$|d\lambda_{im}| = |d\lambda_{im}/d(im)| \cdot d(im)$ appearing in the equation is the absolute value of the hazard curve’s derivative multiplied by $d(im)$. The conditional probability $P[DS = ds_j|im]$ is obtained through the fragility curves providing the probability that the damage state, DS, exceeds its j th value, ds_j , given the intensity measure, that is, $P[DS \geq ds_j|im]$. (Fig. 1—centre). In some cases, an asset’s fragility is derived by studying the response of its components. In such cases it is useful to also define appropriate damage states of asset components, DSCs (e.g. based on the percentage of failed roof covering). $G_{L|DS,IM}(l|ds_j, im)$ is the conditional probability of exceeding a loss value and it can be obtained from the complementary cumulative distribution function of the loss given the j th DS computed for the value l . In PBEE, the loss is typically considered conditionally independent of IM given DS. This means that the loss depends only on the damage of the overall asset and not on the characteristics of the extreme wind phenomenon, i.e. $G_{L|DS,IM}(l|ds_j, im) = G_{L|DS}(l|ds_j)$. The set of values $G_{L|DS}(l|ds_j)$, $j = 1, \dots, n_{ds}$, can be seen as a representation of the exposure for the asset of interest. Finally, n_{ds} is the number of DS.

Using the exceedance rate as the risk metric is useful because, under some conditions, it can be seen as characterizing a homogeneous Poisson process, thus the probability of exceedance of the loss threshold, in any time interval, $P[L(t, t + \Delta t) > l]$, can be readily computed via the exponential distribution as $P[L(t, t + \Delta t) > l] = 1 - e^{-\lambda_l \Delta t}$.

An alternative risk metric is the expected loss in unit time (Fig. 1—right), $E[L]$, which, under some hypotheses, can be computed as:

$$E[L] = \int_{IM} \sum_{j=1}^{n_{ds}} E[L|DS] \cdot P[DS = ds_j|im] \cdot |d\lambda_{im}| = \int_{IM} E[L|im] \cdot |d\lambda_{im}| \quad (2)$$

where $E[L|DS]$ is the expected loss given the DS. An alternative formalization of the expected loss involves the definition of the vulnerability function, $E[L|im]$, that can be computed as:

$$E[L|im] = \sum_{j=1}^{n_{ds}} E[L|DS] \cdot P[DS = ds_j|im] \quad (3)$$

The vulnerability function directly relates the expected loss for the asset of interest to the intensity measure. The approach to risk assessment via vulnerability curves is typical of those cases where this information is obtained via empirical data (Friedman 1975, 1984; Hendrick and Friedman 1966; Leicester and Reardon 1976), while the approach explicitly using fragility functions is more often used when the risk assessment is based on modelling and simulation of the response of the asset under consideration (FEMA 2005; Henderson and Ginger 2007; Vickery et al. 2006a, b; Vickery et al. 2006a, b). This issue will be further discussed in Sect. 2.2.

The approach shown in the equations above, originally developed for earthquakes, can be applied to wind (or any other hazard), if the suitable terms appearing in the equation are available. However, one of the main systematic differences between PBEE and PBWE is that in the former the losses, although possibly coming from structural and non-structural components, are computed referring to a model of the whole system whose main element is the load-carrying structure (e.g. the resisting system of a building). In the latter, especially in case of low- and mid-rise buildings, the interaction of wind with some (mainly non-structural) components directly more regarded (Konthesingha et al. 2015; Pinelli et al. 2004), to a point that the main load-carrying structure can be neglected in the risk assessment. According to the existing literature (e.g. Gumaro et al. 2022), the most important

components for wind risk assessment (main components hereafter) are those pertaining to the building’s envelope, that is the roof covering (RC), roof structure (RS), envelope openings (EO), and envelope walls (EW).

In the case the loss is determined via vulnerability/fragility models for the components, similar to consolidated procedures used in seismic risk assessment (FEMA 2012), the risk is formalized as:

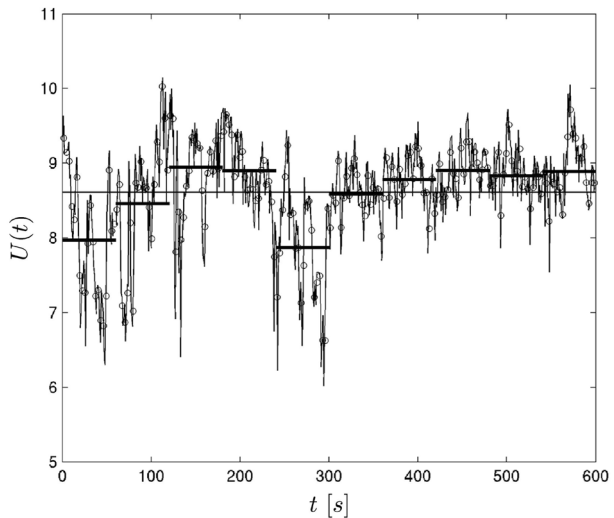
$$E[L] = \int_{IM} \sum_{j=1}^{n_{ds}} \sum_{m=1}^{n_{dsc}} E[L|DS_j] \cdot P[DS = ds_j | \mathbf{DSC} = \mathbf{dsc}_m] \cdot P[\mathbf{DSC} = \mathbf{dsc}_m | im] \cdot |d\lambda_{im}| \tag{4}$$

The **DSC** vector is defined as the collection of damage states of the vulnerable building components to wind and n_{dsc} is the number of its possible realizations. Equation 4 has been developed in the same hypotheses of Eq. 1, also assuming loss dependent only on the whole building DS and the latter dependent only on the damage states of its components, i.e. $E[L|DS, \mathbf{DSC}, IM] = E[L|DS]$ and $P[DS = ds_j | \mathbf{DSC} = \mathbf{dsc}_m, im] = P[DS = ds_j | \mathbf{DSC} = \mathbf{dsc}_m]$, respectively.

2.1 Hazard

Extreme wind hazard is usually provided through hazard curves defining, for a value of an event’s intensity measure im , its (annual) rate of exceedance at the site of interest, λ_{im} . The IM is typically related to wind velocity. Over the years, the definition of wind speed has evolved until the current well-established separation of wind speed into its mean and turbulent (gust) components (Solari 2017). Most standards and building codes (e.g. ASCE 2002; SAA 2002) use, as intensity measure for wind actions for the purpose of building design, the gust (or peak) wind speed, \hat{U}_τ , rather than the mean value, \bar{U}_T . In a record of a given duration, while \bar{U}_T is the mean value of wind speed averaged over a time interval T , \hat{U}_τ is defined as the maximum value of wind speed averaged over a (usually short) time interval τ . Figure 2 is used to illustrate this concept on ten minutes wind speed history recorded by

Fig. 2 Example of different averaging times: 1-s (thin solid line), 3-s (open circles), 1-min (thick horizontal bars), and 10-min (horizontal line); adapted from (Harper et al. 2010)



a sonic anemometer in Western Australia a fixed height. The thin line represents the record data averaged over one-second consecutive time intervals, the open circles over 3-s time intervals, the thick horizontal bars over one minute, and the thin horizontal over 10 min. The same record shows a one-minute (1-min) gust wind speed of about 9 m/s, i.e. the maximum value between the thick horizontal bars (the one between 100 and 150 s), and a 3-s gust wind speed (open circles) of about 10 m/s.

The evolution in IM definition is also reflected in the literature, in terms of hazard curves and vulnerability models (e.g. fragility curves) developed over the years. Currently, the most frequently used intensity measure in wind engineering applications is the 3-s gust wind speed at 10 m aboveground (e.g. Lee 2004; Zhang et al., 2014).

Wind hazard assessment is typically based on three elements: a catalogue of past events, orography, and roughness data. Since simulation techniques calibrated on currently available databases are often used to define wind speed of the rarest events (Yamin et al. 2014), given the probabilistic nature of the intensity measure, a complete and exhaustive catalogue of extreme wind events is essential. Furthermore, since orography and roughness are involved in the definition of wind speed, digital elevation models (DEMs) as well as georeferenced land use data (Tan and Fang 2018), whether natural (vegetation) or influenced by humans (urban environment), represent relevant information.

Usually, wind hazard curves are provided on a regional and global scale under the form of hazard maps each referring to a given exceedance return period. For relatively large wind speed thresholds, the number of observed annual exceedances is generally considered Poisson distributed (Hangan and Kareem 2021; Palutikof et al. 1999). In such a case, the reciprocal of λ_{im} is the average time between consecutive events causing exceedance of the intensity measure of interest, or the return period. The following subsections present and discuss two available hazard maps of tropical cyclone and tornado events, which are embedded in ERMESS as the hazard component of the risk assessment.

2.1.1 Tropical cyclones

On a global scale, freely available tropical cyclone wind hazard maps have been developed in the context of the United Nation International Strategy for Disaster Reduction (UNISDR) Global Assessment Report (GAR) on Disaster Risk Reduction of 2013 (CIMNE 2013; UNISDR 2013). The supporting PREVIEW Global Risk Data Platform (<https://preview.grid.unep.ch/>—last accessed on 19 July 2022) provides these hazard maps for five return periods (50, 100, 250, 500, and 1000 years) with a spatial resolution of one minute (Fig. 3). GAR maps are built on historical data collected at the global scale from various meteorological agencies and grouped in the National Oceanic and Atmospheric Administration (NOAA) International Best Track Archive for Climate Stewardship (IBTrACS) database (Knapp et al. 2010). For each return period, these maps provide 5-s gust wind speeds at 10 m, calculated via a simulation-based technique. The aspects of topography and terrain roughness in the definition of wind speeds have been taken into account through the use of NOAA, a 1-min resolution DEM (Amante and Eakins 2009), and information on land use (Bicheron et al. 2006), respectively.

Given the definition of a hazard map for the five aforementioned return periods, it is possible to define a hazard curve for each site via interpolation. In addition to wind speed, hazard modelling of tropical cyclones in a more extensive risk analysis should include related phenomena such as storm surge and precipitation (Cardona et al. 2014). However,

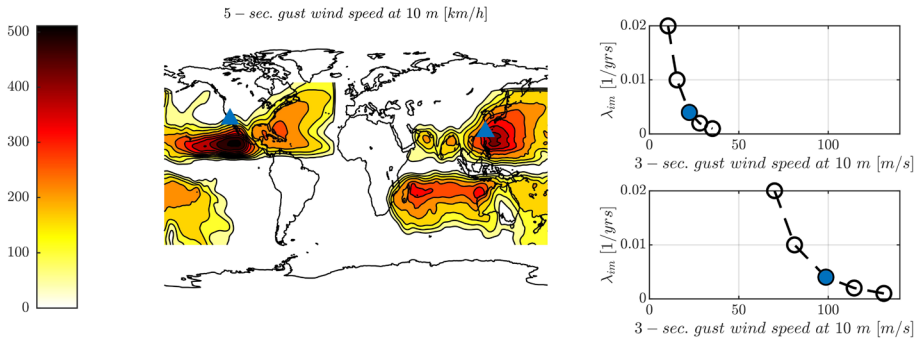


Fig. 3. 250 years return period tropical cyclone hazard map (left) and hazard curves (right) for two sites: Los Angeles (top) and Taipei (bottom)

to date, there are no current studies that consider this aspect on a global scale (Ward et al. 2020).

2.1.2 Tornadoes

The few existing studies about tornado hazard are regional and are mainly based on insurance companies’ claims data and therefore not readily accessible. North America is a region particularly affected by tornados (Goliger and Milford 1998), and some dedicated studies are available. The NOAA Storm Prediction Center database (about 60,000 events since 1953) has motivated attempts to develop simulation-based tornado hazard maps at different scales (e.g. Fan and Pang 2019). These tornado hazard maps adopt the Enhanced Fujita (EF) scale (WSEC 2004) intensity levels that have evolved from the Fujita (*F*) scale (Fujita 1970) developed in 1973 based on the observed damage. This scale defines six levels of event intensity, from EF0 to EF5 and can be loosely seen as analogous to macroseismic intensity scales for earthquakes (ESC 1998). Based on qualitative degrees of damage suffered by the built environment and even vegetation, the EF-scale defines ranges of 3-s gust wind speed associated with each intensity level Table 1.

For each grade of the EF-scale, US hazard maps were developed (Standohar-Alfano and van de Lindt 2015) based on the NOAA Storm Prediction Center database. (Although some of the data were excluded given the creation of a reference scale only in the 1970s, about 40,000 events were considered over a span of time of about 40 years.) Developed for

Table 1 Enhanced Fujita scale

EF	Damage description	3-s gust speed at 10 m [m/s]
0	Light	29–38
1	Moderate	39–49
2	Considerable	50–60
3	Severe	61–74
4	Devastating	75–89
5	Incredible	≥ 90

different spatial resolutions (2, 1, and 0.5 degrees), these maps define the annual probability of experiencing an EF0–EF5 wind speed in the continental USA (Fig. 4).

These maps can also be interpreted as the rates of occurrence of the considered EF grade at any point in the USA. Due to the discrete intensity scale, the hazard curves that can be obtained from them exhibit stepwise variations of rate versus intensity. However, a dedicated study (Masoomi and van de Lindt 2016) proposed a second-order exponential function to fit the data in log–log space, according to the following formulation (for $IM \geq 22$ m/s):

$$\ln G_{IM}(im) = \alpha \cdot e^{\beta \cdot \ln(im)} + \gamma \cdot e^{\delta \cdot \ln(im)} \quad (5)$$

with α , β , γ , and δ being parameters and $G_{IM}(im)$ the complementary cumulative distribution of the annual maximum 3-s gust wind speed.

2.1.3 IM conversion

Because the definition of wind speed intensity measures has varied over the years, procedures have been developed for intensity measure conversion. For example, since the GAR hazard maps are referred to τ equal to five seconds, it is possible to convert their values to a reference value of three seconds. To this aim, the Engineering Sciences Data Unit (ESDU) (Vickery and Skerlj 2005) conversion method can be employed. The ESDU approach to intensity measure conversion was developed for extra-tropical cyclone conditions; however, comparison of tropical cyclone conditions real data with the one provided by the ESDU model suggests that the latter can also be applied for these events.

The hypothesis at the basis of the model lies in the assumption of cyclonic wind flow near the ground (up to 50–100 m) be described by the standard boundary layer theory. Under this assumption, considering a logarithmic profile for the 1 h (3600 s) mean wind speed, \bar{U}_{3600} , the peak wind speed referred to a certain gust averaging interval τ is described by the definition of the of the gust factor, $G_{\tau, 3600}$, as the ratio between \hat{U}_{τ} and \bar{U}_{3600} . However, the method involves an iterative procedure and does not allow the conversion for averaging times different from 3600 s for mean wind speed. A simplified method that does not involve iterations was developed by the WMO (Harper et al. 2010). This approach, in addition to introducing an approximation in the longitudinal turbulence intensity definition for the gust factor assessment, also allows the definition of mean wind speed for averaging

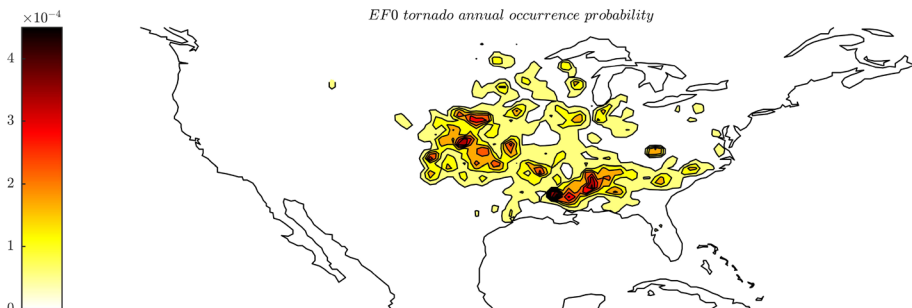


Fig. 4 Tornado hazard map

time intervals T , different from 3600 s. The gust factor $G_{\tau,T}$ can be defined for T different from 3600 s, through the G_T function defined as:

$$G_T = \frac{G_{\tau,T}}{G_{\tau,3600}} = \frac{\bar{U}_{3600}}{\bar{U}_T} \approx 0.2193 \cdot \ln [\log (T)] + 0.7242 \quad (6)$$

2.2 Vulnerability and fragility

Wind vulnerability of a building or component is usually represented by the expected value of the loss as a function of the intensity of the hazardous phenomenon. Building vulnerability functions to extreme winds were initially introduced as a risk assessment tool by the insurance industry in the 1960s and have been subject to considerable development since then. However, the trend is recently shifting towards the development of fragility functions that provide the probability of reaching or exceeding some performance level given intensity. Then they can be combined with different loss models and are more adaptable to the specific case being considered.

Literature approaches for building vulnerability and fragility assessment can be classified into three categories: (i) regression of loss data against intensity measure collected from post-event insurance claims or surveys (Friedman 1975, 1984; Hendrick and Friedman 1966; Leicester and Reardon 1976); (ii) expert judgement (i.e. heuristic) (Hart 1976; Pita 2015; Wehner et al. 2010); (iii) quantitative assessment of the physical damage sustained by the building and its components (CIMNE 2013; FEMA 2005; Sciaudone et al. 1997; Unanwa et al. 2000; Vickery et al. 2006a, b; Vickery et al. 2006a, b). Usually (i) is more devoted to developing vulnerability functions while (ii) and (iii) are more often fused to develop fragility curves. However, these boundaries are not rigid; for example, the engineering approach often involves advanced simulation of wind-environment-building interactions, and the resulting damages are converted to monetary losses by actuarial principles.

There are several differences between these models, ranging from the level of complexity involved in their development, to the treatment of uncertainty. Empirical models exhibit limited exportability for risk assessment purposes because they are based on data that refer to regions with their own specific characteristics. Heuristic and engineering-based models are flexible, because the differences in local construction practice and building codes can be explicitly accounted for in the vulnerability or fragility modelling; however, features such as modelling of uncertainties and interactions between building components, which empirical models implicitly incorporate, need explicit consideration. The engineering approach enables the development of models for specific assets, such as buildings, which is something that claims cannot readily capture due to the need of pooling possibly heterogeneous data. However, this requires effort and expertise in numerical modelling and analysis, which may not always be available. It should be also mentioned that categorization of these approaches is not always as clear cut as implied by this brief discussion; for example, early engineering-based methods were also integrated with expert judgement and insurance claims and are sometimes used within heuristic approaches to calibrate specific vulnerability models (e.g. Henderson and Ginger 2007).

Some recent research effort has been looking at detailed wind fragility study of some building components (e.g. Lee 2004; Sparks et al. 1994; Zhang et al. 2014), because, as already discussed, wind-related building losses are mostly due to failures of the components that constitute its outer cladding, or envelope. For example, (Fig. 5) shows a

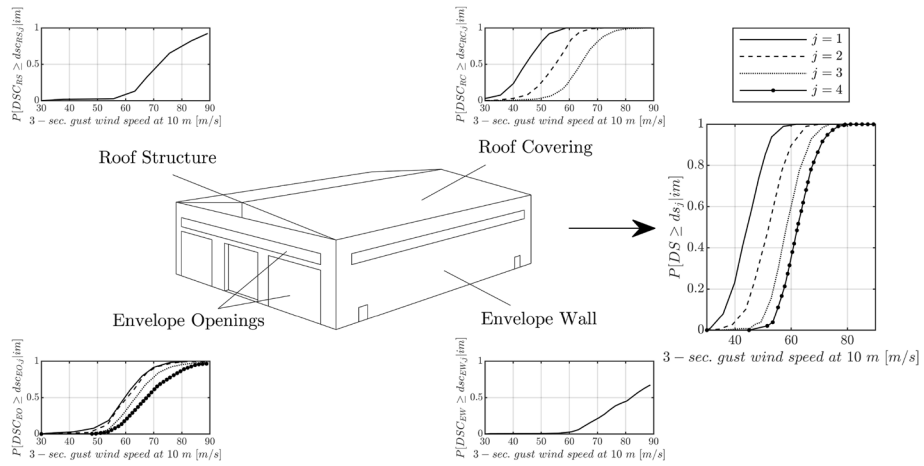


Fig. 5 Outline of building fragility composition (adapted from FEMA 2005)

schematic building representation where these principal components RC, RS, EO, and EW are identified. The figure also shows a series of fragility functions per component that are all expressed in terms of the same IM, in this case 3-s gust wind speed at 10 m, and the resulting building-level fragilities. On a side note, many of these studies derive the fragilities of single components by considering different openings scenarios of the building envelope, for example, by considering wind actions on the roof according to code-based procedures that discriminate between dominant or non-dominant opening scenarios (ECS 2005).

On these bases, the trend in the last two decades in the context of risk has turned in the direction of expressing the vulnerability of buildings through their component fragility functions via compositional methods. There is a variety of such approaches, from fault tree analysis to fluid–structure interaction simulation. This enables studies to delve into higher levels of detail, going as far as the consideration of component fragility curves for such elements as roof fasteners (Konthesingha et al. 2015).

2.3 Exposure

The loss assessment has received much more attention from the insurance industry than the engineering community (Mason and Parackal 2017). According to the common separation of the losses in direct and indirect, the focus has been more directed towards the former, due to the complexity and modelling challenges of the latter. In fact, indirect damage can be described as an immaterial or delayed (with respect to the hazardous event) damage, like the business interruption or the need of alternative accommodations for families whose home has been damaged. In case of buildings, direct loss is usually intended as repair or replacement costs of damage, or damage to content, (e.g. water penetration following the opening of breaches in the building envelope (Lee and Rosowsky 2005; van de Lindt and Dao 2009); therefore, it is more apt to be quantified from the engineering point of view. For these reasons, in line with the data most readily available from the literature and the insurance industry, this study, and then ERMESS, only focuses on direct losses. A common measure of these losses is the damage ratio, DR, i.e. the ratio between the direct loss

Table 2 Expected damage ratio as a function of building damage state for residential and commercial occupancy

Building damage state	$E[DR DS]$	
	Residential	Commercial
0	0.00	0.00
1	0.25	0.15
2	0.50	0.25
3	0.70	0.30
4	1.00	0.45

suffered by the building to its insured value, IV_s . The expected value of damage ratio given the building DS, $E[DR|DS]$, is usually provided by insurance companies, based on a large number of claims, according to the occupancy (Table 2 Dr. Fabio Petruzzelli, AXA-XL, written communication). When the insured value is known, the building loss in monetary terms can be evaluated as $E[L] = IV_s \cdot E[DR]$.

3 Database and taxonomy

One of the core elements of the study herein presented is the compilation of a database of vulnerability and fragility curves of buildings, components, but also elements, collected from the literature. For practical purposes, the database has been separated into a fragility database, collecting only fragility curves and a vulnerability database, collecting only vulnerability curves, according to the distinction made in Sect. 2.2. The entire database contains a total number of 5228 fragility and 272 vulnerability curves from about 30 different academic and technical sources. A considerable part of the fragility database is represented by the 4588 curves from the FEMA HAZUS-MH 2.1 Technical Manual. The FEMA developed fragility curves for different typology of building and occupancy, from residential to commercial. For each category, HAZUS provides nonparametric fragility curves for the whole building but also at the component level. Since in 2022 all these curves have been digitized and parameterized through fitting lognormal cumulative distributions (Ascolese 2022), their data were incorporated into the fragility database. As shown in (Fig. 6), about one-third of the fragility database is made of curves for buildings, 67% by building component curves, and less than 1% by element fragilities. In the vulnerability database, 11% of the curves are related to building components while the remaining are building vulnerability curves.

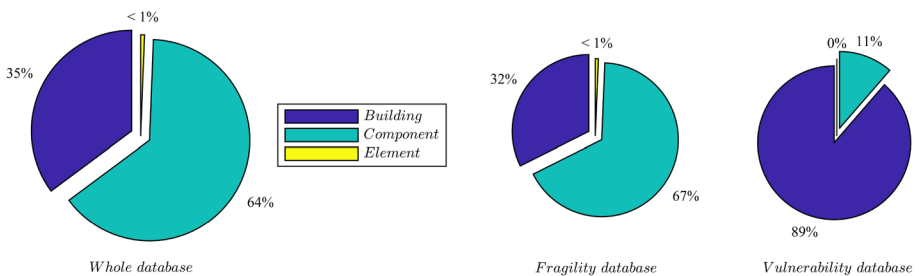


Fig. 6 Databases population

The relational database has been developed as a MATLAB® structure (The MathWorks 2020) a type of data object whose *fields* correspond to ad hoc defined taxonomy entries. This taxonomy, as discussed in the following, serves to filter and select curves (i.e. records) for the risk analysis. It has been developed based on the study of relevant extreme wind risk analysis literature and clustered according to the following field groups: *Data*; *Source*; *Site*; *Building*; *Damage state*; *Roof*; *Roof covering*; *Envelope wall*; *Envelope openings*; *Curve measures*; *Other*; others (Fig. 7). However, it is important to note that, because the taxonomic entries were conceived to cover as much information related to extreme wind response as possible, not every field is always applicable to all the curves present in the database. This is especially true for models from older sources, for which some entries must necessarily remain null. The IM and *values* fields contain two vectors of equal length, with the first being a set of discrete IM values and the second being the corresponding ordinates of the fragility or vulnerability curve of the specific entry. The *notes* field is needed for the inclusion of clarifications or other relevant information that may be deemed too case-specific to deserve a dedicated taxonomic entry. The last group entry of this field, *metadata*, collects the parameters of the distribution form, in cases where a parametric model has been fitted.

The source field group collects the taxonomy entries needed to identify the study from which the fragility or vulnerability curves have been extracted and some main

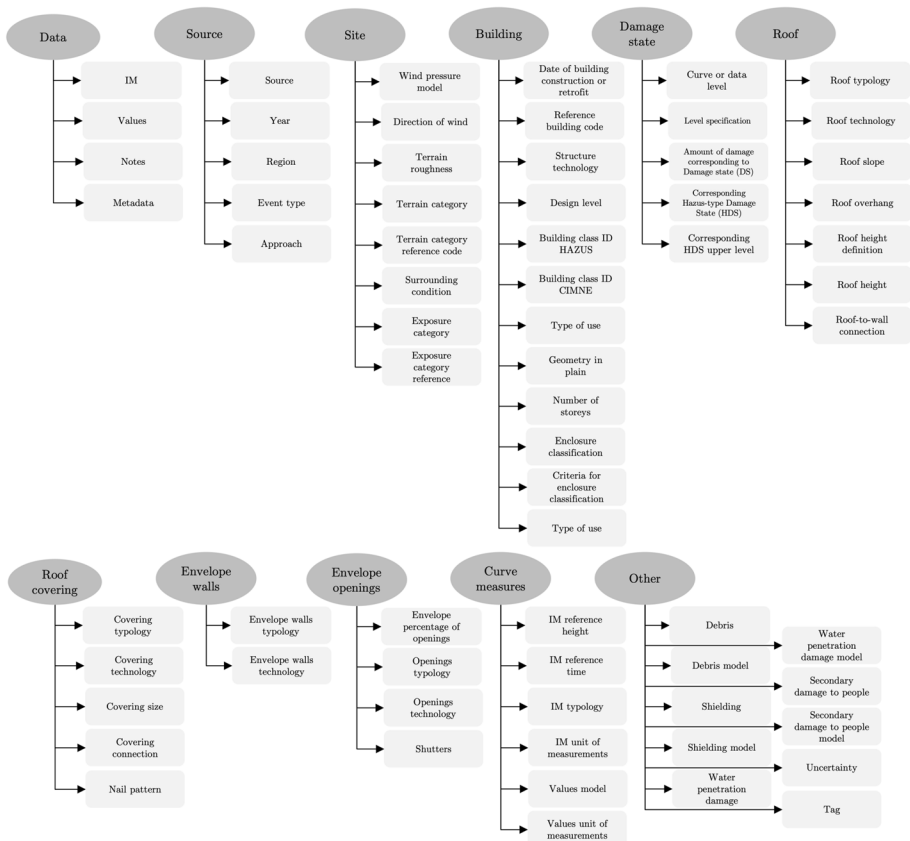


Fig. 7 Taxonomy entries according to the field groups

features. Then, the first taxonomic entry, *source*, concerns a tag composed according to an Author(s)_Year scheme (e.g. Henderson_Ginger_2007 or Li_Ellingwood_2006). The following entries define the *year* of the study publication and the *region* of interest, defined according to the nation for which the considered model was developed. Furthermore, given the different features of the extreme wind phenomena, it was considered necessary to link each curve to the type of event for which it has been developed (e.g. a tropical cyclone or tornado) through the definition of its *event type* value. Finally, the last entry of this field group concerns the *approach* used for the development of the curve according to the classification addressed in the previous discussion: past loss data, heuristic, and engineering-based.

The third field group, *site*, concerns the local features that influence the local wind field and the loads on structures. The *wind pressure model* taxonomy entry defines the employed model for conversion of local wind speed into pressure on structures, e.g. the ASCE Standard 7–02 or the Tokyo Polytechnic University aerodynamic database (TPU 2007). Moreover, as discussed previously, wind *direction* and *terrain roughness* can also affect the definition of the local wind field and loads on the structure and have been therefore included as record entries. However, because the definition of terrain roughness (typically in units of length) may vary between national standards, codes, and other sources, the fields *terrain category* and *reference code* were included to accommodate potential disparity. Additionally, some codes do not actually define terrain features but rather a level of the site exposure, for which case the *surrounding conditions*, *exposure*, and the *reference code* fields were added.

Once the site characteristics have been defined, it is possible to move on those of the *building*. *Date of building construction* and *reference building code* are entries intended to link the building to a specific date and design practice, respectively (e.g. PCI 1971). These two building-related taxonomic entries, in conjunction with the *design level* entry that defines a quality rating for structural detailing (e.g. high, medium, low), can be useful for filtering the fragility/vulnerability databases to identify models suitable for representing different conditions of construction. The following entries define some broad characteristics of the building: two building class IDs follow the codifications provided by HAZUS and CIMNE, respectively; *technology* records construction material and elevation (e.g. high-, mid-, or low-rise wood frame or masonry); *type of use* defines the occupancy (e.g. residential or commercial), while *geometry in plan* and *number of stories* define geometric characteristics of the building. Then, two taxonomy entries are dedicated to the *enclosure classification* (e.g. enclosed or partially enclosed) and its *criteria*, since modern standards usually classify the actions on the building following the definition of openings configuration, widely accepted as a key parameter in the determination of wind pressure.

In order to apply the fragility composition approach described in the next section, the curve (or data)-level entry defines a vulnerability or fragility curve first detail level between whole building, building component, or building component element, while level specification defines a second (e.g. roof tile, roof sheathing, or envelope opening). The following entries define, where applicable, the amount of damage for which the fragility curve has been developed, corresponding to the *HAZUS-based damage state* (HBDS), i.e. the DS definition provided by HAZUS and which in some cases has been slightly generalized. (Details are provided by Pandolfi 2022.) Then, the numerical corresponding HBDS and, in the case of components and elements, the numerical HBDS corresponding to the building or the component, respectively.

The roof is widely recognized as the most vulnerable building component for wind risk analysis (e.g. Qin and Stewart 2019, 2020). For this reason, more detailed taxonomy entries are provided. Roof typology provides a first level information (e.g. hip or gable roof) along with its technology (e.g. wood frame). Then, subsequent entries allow the definition of more details, such as slope, the presence or not of overhangs, height, and type of connection with the envelope walls (roof-to-wall connections field).

The *roof covering* field group defines the characteristics of this main component by defining of the type (e.g. panels or tiles), technology (e.g. metal or wood panels), element size, connection type (e.g. type of nails), and connection pattern (e.g. the nails' spatial arrangement, if applicable). The study of this component is essential for the roof damage definition but also for the debris action, since the roof covering is known as one of its main sources.

The taxonomy entries related to the *envelope walls* are the typology (e.g. unreinforced or reinforced masonry) and technology (e.g. metal sheeting or timber panels). These taxonomy entries are less detailed with respect to the ones pertaining to the roof, as envelope walls are comparatively less vulnerable to extreme winds. However, the same cannot be said for *envelope openings* whose failure, due to wind pressure but also to debris impact, is one the main sources of increase in internal pressure and, as a consequence, of the potential for progressive failure of the structure. A first field for its characterization is the percentage of openings on the building envelope since; for example, the probability of debris impact increases with opening size. Other taxonomy entries are related to opening typology (e.g. glass doors or windows), technology (size and thickness), and the presence of shutters (e.g. jalousie).

Then, the *curve measures* field group refers to the intensity measure and the related vulnerability measure of each record. Since the previous discussion highlighted the importance of the different features in the definition and conversion of IM, the related taxonomic entries provide the definition of reference height (e.g. 10 m), reference time (e.g. 3-s or 10-min), typology (mean or gust) and units (e.g. m/s or mph). Regarding the vulnerability measure, the entries values model (e.g. discrete or parametric) and values unit of measurement (e.g. MDR or probability of exceeding a DS) are defined.

The last taxonomic entries labelled as *other* include various information useful for risk assessment that do not fall into one of the preceding fields. First, taking *debris* impact into account in the development of fragility and vulnerability curves can be important in some situations, especially in a residential environment. A number of different models have been developed to study this phenomenon and are collected under the field *debris model* (e.g. Lin and Vanmarcke 2008). Also the *shielding* effect of the structure, that is, the protection provided by nearby buildings, the *damage due to water penetration* from the breaches that occur in the envelope, and the *secondary damage to people* are characteristics that some authors deem necessary for the definition of extreme wind vulnerability. Therefore, for each of these aspects two taxonomic entries are considered, the first describing whether this phenomenon has been taken into account, while the second describes the employed *model*, if any. The last fields are used to account for the possibility that the authors of the record have explicitly modelled *uncertainties* in the development of their results and to assign a *tag* (i.e. primary key) to each record for its unambiguous identification into the database.

It is important to mention that the same taxonomy entries are used both when the record refers to the whole building and when it refers to a single component or element. This is because some characteristics of the building may be relevant information pertaining to one of its components or elements and vice versa. This is due to the interaction between the

component failures, i.e. the progressive damage, that is a key factor in the reliable assessment of their wind vulnerability. For example, in the analysis of the fragility of the roof or the whole building, it is important to take into account the characteristics of the openings of the envelope since their failure implies an increase in the internal pressure of the whole structure. It should also be highlighted that, although this plethora of taxonomic entries is intended to assist the user in filtering the databases, that is isolating groups of potentially suitable fragility or vulnerability models for each case of risk analysis, the responsibility for the actual choice of the model ultimately resides with the analyst.

4 Fragility composition

The fact that the unit asset of interest in portfolio risk assessment is the building, and thus consequence models are typically available at the building level, while many fragility models are available at the component level, motivated the development of methods to compose component-level fragilities into building-level ones. These methods, for example those based on fault tree analyses (Gangloff 1974), can be considered approximate, yet are more resource-effective than fragility development based on modelling the entire building system and the interaction between damage to its components, i.e. the so-called damage propagation. However, available fragility composition methods can be very case-specific, as in the case of Unanwa et al. (2000), and/or require some degree of expert judgement for their implementation. In this context, an ad hoc fragility composition procedure, consistent with the PBWE framework, was developed and embedded in ERMESS.

This method requires the definition of a building-specific damage matrix that associates the (global) damage states of the entire asset to those of its components. An example of a damage matrix, appropriate for residential buildings, is provided in Table 3. The rows of the matrix correspond to the global damage states and the columns to the components. Each bold entry in the matrix contains a damage condition for the corresponding component that is sufficient for the entire asset to be designated at that row's DS, for the example shown in the table, which corresponds to a residential building, which can be claimed to have sustained minor damage if any single fenestration has failed, or if a percentage of roof cover elements between 2 and 15% have failed (or if both components have experienced that extent of damage), according to the second row of the matrix. The concept of a damage matrix has been used in the past by several authors (e.g. Griffis et al. 2013; Hart 1976), while the most comprehensive and detailed collection of wind-related damage matrices at the time of writing is provided by FEMA, in the context of the HAZUS project (Vickery et al. 2006a, b; Vickery et al. 2006a, b).

The fragility composition method developed for ERMESS uses a more parsimonious, numerical version of the damage matrix. In this matrix, each component's damage states are numbered starting from zero and in ascending order with damage severity. Note that each component follows its own DSC numbering, which may be different from that of the asset's/building's DS. With this formalization, all elements of the damage matrix are replaced by a numerical DSC value, yet retaining the same significance as before, regarding the definition of the asset DS from the condition of its components; for example, this substitution applied to the damage matrix of Table 3, results in the numerical matrix shown in Table 4.

Thus, denoting the element of the numerical matrix at the j th row and k th column as dsc_{jk} , with $j = 1, 2, \dots, n_{ds}$ and $k = 1, 2, \dots, n_c$, and DSC_k the random variable

Table 3 Damage matrix for a residential building (adapted from FEMA 2005)

Building damage state (number and description)	Roof cover failure	Window/door failures	Roof deck failure	Roof structure failure	Wall structure failure
0 (No damage or very minor Damage)	≤ 2%	No damage	No damage	No damage	No damage
1 (Minor damage)	> 2% and ≤ 15%	One window, door, or garage door	No damage	No damage	No damage
2 (Moderate damage)	> 15% and ≤ 50%	> 1 and ≤ the larger between 3 and the 20% of the total	1 to 3 panels	No damage	No damage
3 (Severe damage)	> 50%	> the larger between 3 and 20% and ≤ 50%	> 3 and ≤ 25% of the total	No damage	No damage
4 (Destruction)	Typically, > 50%	> 50%	> 25%	Yes	Yes

Table 4 Numerical matrix from the damage matrix of Table 3

Building DS	Roof cover	Window/door	Roof deck	Roof structure	Wall structure
0	0	0	0	0	0
1	1	1	0	0	0
2	2	2	1	0	0
3	3	3	2	0	0
4	3	4	3	1	1

representing the *k*th component’s damage state, then the fragility function for the *j*th damage state of an exposed system can be computed as:

$$P[DS \geq ds_j | im] = 1 - \prod_{k=1}^{n_c} \{1 - I(dsc_{jk}) \cdot P[DSC_k \geq dsc_{jk} | im]\} \tag{7}$$

In the equation, $I(dsc_{jk})$ is an indicator function that returns 1 if the element dsc_{jk} of the numerical matrix corresponds to a component damage condition that is sufficient for the declaration of the entire asset at the corresponding DS (in other words if the element of the matrix is set in bold type), and 0 otherwise. The terms $P[DSC_k \geq dsc_{jk} | im]$ are calculated from each component’s fragility functions. This formulation assumes that for all DS of the exposed asset $P[\bigcap_{k=1}^{n_c} (DSC_k < dsc_{jk} | im)] = \prod_{k=1}^{n_c} P[DSC_k < dsc_{jk} | im]$, that is conditional independence, given $IM = im$, of each component’s probability of being in a DSC. Although this hypothesis could sound counter-intuitive, due to the well-known interaction between component failures, other works have also explored similar assumptions (Filliben et al. 2002; Pinelli et al. 2004).

In order to experiment on the level of approximation introduced by this assumption, the following example calculation is carried out: a damage matrix and the associated fragility curves are selected from the HAZUS technical manual, for an industrial building (typology G.1 according to FEMA 2005). This choice is motivated by the fact that HAZUS itself also provides whole building fragility curves obtained through numerical simulation; therefore, these curves can be used to investigate the accordance of the curves resulting from the proposed composition approach with those obtained via simulation of the building’s response to wind. The corresponding numerical matrix is shown in Table 5, and the component fragilities are plotted in Fig. 8.

Implementation of Eq. 8 for all damage states of the building, it is possible to calculate its fragility curves via the composition approach, shown in Fig. 9. This figure also shows the comparison with fragility curves provided by HAZUS via its engineering simulation-based approach. It is possible to observe that the presented composition-based

Table 5 Numerical damage matrix for an industrial building (HAZUS typology G.1)

Building DS	Roof cover	Roof deck	Joist	Doors	Wall
0	0	0	0	0	0
1	1	0	0	1	0
2	2	1	0	2	0
3	3	2	1	3	1

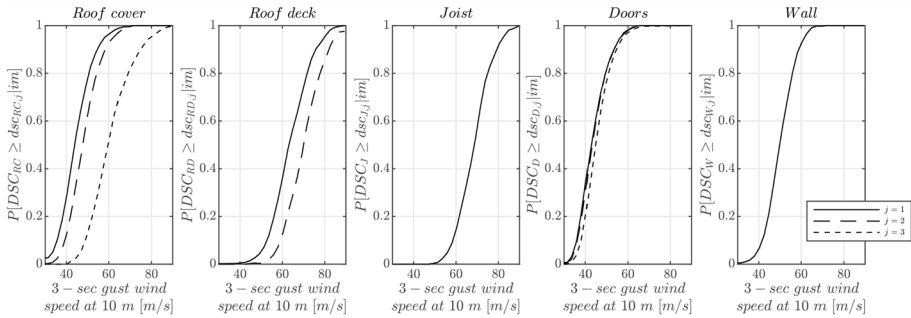
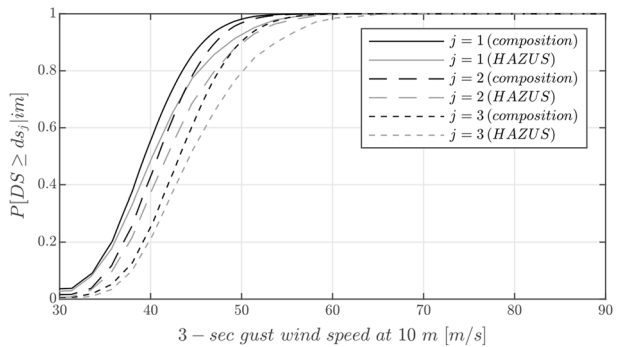


Fig. 8 Building component fragility curves for industrial building (typology G.1), adopted from FEMA (2005)

Fig. 9 Industrial building fragility curves comparison



approach returns the results with a certain degree of agreement with those provided by HAZUS simulation, with a maximum difference of about 0.1, and with discrepancies being larger at the more severe building DS and for wind speed ranging between 90 and 120 mph. A more circumspect comparison, in terms of predicted losses, will follow later in the text.

5 ERMES graphical user interface

The architecture of the ERMES’ GUI reflects the subdivision of the PBWE approach to risk calculation into its main components, resulting in three main modules for hazard, vulnerability and exposure, as shown in (Fig. 10). Each main module is, in turn, composed by sub-modules that perform specific operations internally, such as IM conversion or fragility composition. In its upper part, the interface also displays the risk analysis input of for each main module.

After the user definition of the site characteristics (geographical coordinates and terrain roughness) and the type of hazardous event (tropical cyclone or tornado), the hazard module on the left allows the definition of the hazard curve (or the single intensity measure in case of scenario analysis). This definition can be performed via direct user input (.csv file) or by selecting built-in hazard maps described before. Then, the

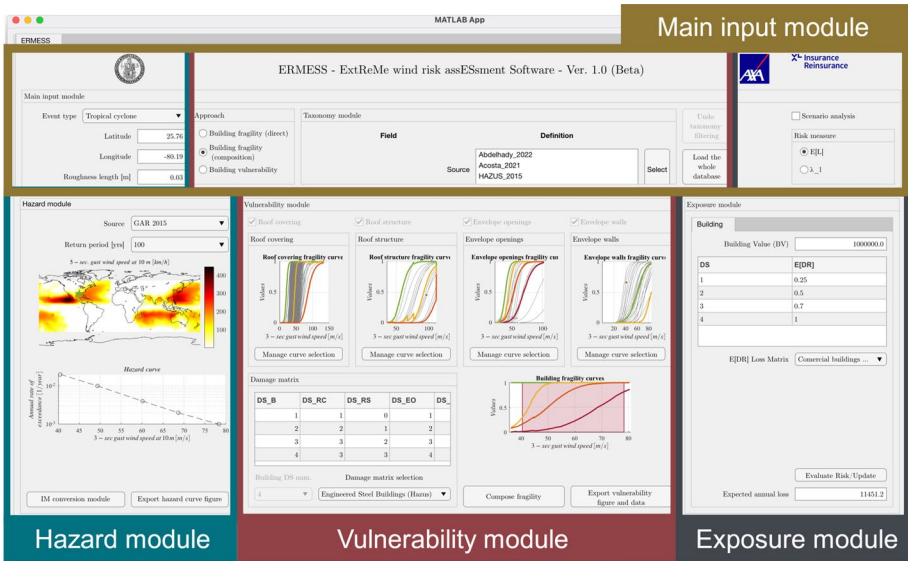


Fig. 10 ERMESS main interface

intensity measure conversion sub-module enables the conversion, if needed, of IM to the reference value of 3-s gust at 10 m.

In the vulnerability module, the input section is dedicated to the choice of the approach to follow in the assessment of vulnerability, which can be performed in three different ways. The first involves the direct selection of the building fragility from the database, the second the selection (or definition via user input) and composition of component fragility, and the third concerns the selection/definition of a vulnerability model. The remaining part of the input section is occupied by the taxonomy sub-module that enables the selection of the database curves of user interest, according to the described taxonomy.

The vulnerability module in Fig. 10, according to the fragility composition approach discussed before, shows a damage matrix panel and four fragility curve selection panels, one for each building main component. Once a damage matrix has been selected among those built into ERMESS, or has been defined by the user (in the latter case for a maximum number of four main component damage states), the definition and management of the component fragility curves is enabled through the dedicated component fragility sub-module, which is shown in Fig. 11, assisting the user in the selection of fragility curves for all damage states defined in the damage matrix. On the right, the panel offers an overview of the selected curves. A sub-taxonomy panel helps the user in filtering and selecting main component.

Figure 11 also shows an application example in which the median fragility curve (green) for roof covering component is selected from those (grey) remaining from the following taxonomic filtering: tropical cyclone event type, open terrain category, HBDS equal to 1, single-family wooden structure with 2 stories, and gable roof technology. This possibility of using the mean or median of several alternative fragility models, can be seen as a way of dealing with epistemic uncertainty on a component or asset. Besides the possibility of

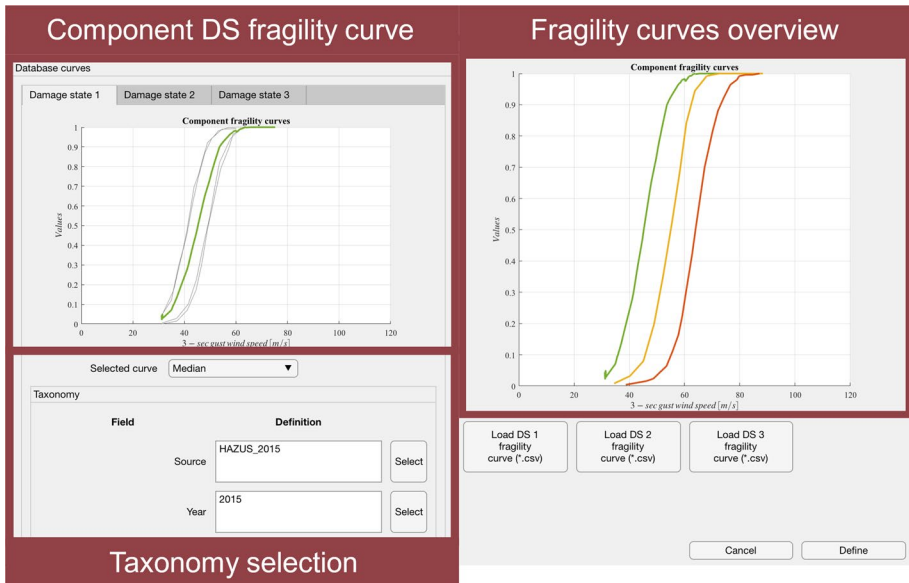


Fig. 11 Building component fragility selection sub-module

selecting fragility curves from the database, ERMESS also allows the uploading of user-defined curves in.csv format.

Once the fragility curves for each main component have been defined or selected, it becomes possible to get the fragility of the building. The output building fragility curves are displayed on a panel that also shows the IM range for which the hazard curve has been defined. In the case of scenario analysis, this range boils down to a single IM value. Knowing the building fragility curves, the risk measures can be defined in the exposure module, given the selection or user definition of appropriate consequence functions, on the right side of ERMESS main interface. In a dedicated input panel, selection of the type of analysis is possible (scenario or not) as well as of the risk measure according to the formulations of Sect. 2. It is worth mentioning that if the fragility or vulnerability curves show no values within the integration limits of the hazard curve, they are set null on the left (low values of IM) and equal to 1 on the right (high values of IM).

5.1 Illustrative application

To show the capabilities of ERMESS and possibly validate the fragility composition method, risk analysis using ERMESS is illustrated in this section, using a building structure that is fictitiously placed in different sites. Three sites are considered for this application, all corresponding to the same open terrain condition, with roughness length equal to 0.03 m, yet subject to different hazards for tropical cyclone type events: high (Taipei, lat. 25.03, long. 21.56), medium–high (Miami, lat. 25.76, long. – 80.19) and low (Los Angeles, lat. 34.05, long. – 118.24). The corresponding hazard curves are shown in (Fig. 1) (Miami) and (Fig. 3) (Los Angeles on the top and Taipei on the bottom).

Table 6 Numerical damage matrix for the illustrative application

Building DS	RC DSC	EO DSC	Roof deck DSC	Joists DSC
0	0	0	0	0
1	1	1	0	0
2	2	2	1	0
3	3	3	2	1
4	3	4	3	2

Table 7 Component fragility parameters

Component	DSC	Residential occupancy w/o windborne debris		Commercial occupancy with mixed missiles	
		μ	σ	μ	σ
		RC	1	4.6835	0.16742
	2	4.7985	0.14382	4.8041	0.14625
EO	1	4.558	0.11115	5.045	0.076709
	2	4.6258	0.10048	5.0587	0.073581
	3	4.849	0.093658	5.1188	0.06548
	4	5.3201	0.081661	5.3554	0.058219
Roof deck	1	4.9743	0.10068	5.0261	0.094656
	2	5.0546	0.089835	5.0982	0.070899
	3	5.3646	0.15602	5.3081	0.10045
Joist	1	5.0623	0.088146	5.1283	0.07373
	2	5.0623	0.088146	5.1283	0.07373

In order to maintain the possibility of comparing loss results, obtained via the approximate building-level fragility composition from those of its components, with results of higher accuracy coming from simulation, the selected building typology is such that the latter results are already available in HAZUS documentation. More specifically, the structure considered at all three sites is a five-storey building, with an envelope characterized by thirty-three per cent glazing coverage and a built-up roof cover technology. At each site, two different possible combinations of building occupancy and debris environment were considered, bringing the total number of cases examined to six: a residential occupancy in surroundings that offer no windborne debris and a commercial occupancy in a mixed commercial/residential environment that may subject the building to windborne missiles such as roof tiles and gravel. The former combination is comparable to the HAZUS designation *F.25* while the latter to *F.26*.

The four main components taken to comprise this type of building are the RC, EO, roof deck, and joists and the building damage states considered are very minor, minor, moderate, severe, and complete damage, labelled as $j=0$ through 4. The building-specific numerical matrix used for the implementation of the fragility composition method in ERMESS is given in Table 6.

For the component fragilities, lognormal parametric models were used, taken from the ERMESS database that collects fragility parameters fitted against HAZUS data, that is:

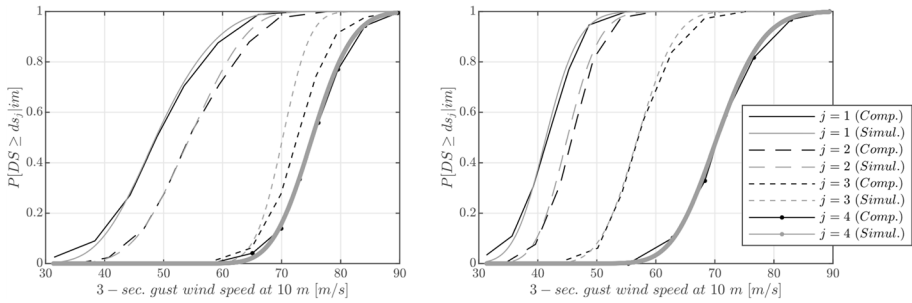


Fig. 12 Category *F.25* (residential—left) and *F.26* (commercial—right) engineered building fragility comparison between simulation and composition approaches

Table 8 Risk analyses results by ERMESS

Site	Hazard	Building typology	Occupancy	Fragility method	$E[L_s][\$]$
Taipei	High	<i>F.26</i>	Commercial	Simulation	7579.5
				Composition	7711.1
		<i>F.25</i>	Residential	Simulation	18116.1
				Composition	18207.5
Miami	Medium–high	<i>F.26</i>	Commercial	Simulation	2942.1
				Composition	4095.3
		<i>F.25</i>	Residential	Simulation	11367.0
				Composition	12465.0
Los Angeles	Low	<i>F.26</i>	Commercial	Simulation	0.3
				Composition	0.9
		<i>F.25</i>	Residential	Simulation	2.8
				Composition	4.4

$$P[\text{DSC} \geq \text{dsclim}] = \Phi\left(\frac{\ln(\text{im}) - \mu}{\sigma}\right) \tag{8}$$

where $\Phi(\cdot)$ is the standard Gaussian function and μ, σ are model parameters that can be found in Table 7.

It should be noted that no fragility parameters are provided for the RC at its third DSC; in fact, the probability that, for this building type, the specific component can be brought to that DSC is considered negligible. Additionally, the fragility parameters for the two DSC of the joist components are identical, meaning that transition into the second from the first is immediate. Implementation of the ERMESS fragility composition procedure provided building-level fragilities for the two occupancy-debris situations into which the building is considered. These curves are presented in Fig. 12, plotted against the corresponding curves developed through simulation in HAZUS. It is recalled that the residential occupancy scenario is to be compared with HAZUS designation *F.25* curves while the commercial with *F.26*. From the figure, it emerges that the greatest difference between corresponding building-level fragilities is observed for DS 3 of the residential occupancy scenario.

These fragility curves, both the ERMESS-developed via component composition and their HAZUS simulation-based counterparts were used in ERMESS to compute expected annual loss, $E[L_s]$. The HAZUS fragilities were fed into the software as user input. The monetary annual loss was calculated considering the expected value of damage ratios from Table 2 for the two occupancy classes, and a building insured value, IV_s , of one million dollars. The $E[L]$ results of these analyses are summarized in Table 8.

Examining the expected annual monetary losses in Table 8, it is possible to observe a difference, normalized to the value relative to the vulnerability obtained by simulation, of less than 2% for the site characterized by high hazard, for both building types. The difference increases as the hazard of the site and the comparability of the curve sets decrease. However, these increased differences are observed for very small annual expected loss values. For medium–high hazard, the difference is limited to the range of about 10–40%.

This validation attempt has shown promising agreement with the results obtained via more accurate methods. However, the applicability of this methodology hinges on the availability and quality of the input component fragility.

6 Final remarks

The presented study was aimed at discussing the technical basis of ERMESS—extreme wind risk assessment software, dedicated for rapid risk assessment of building portfolios to wind hazard. ERMESS is based on the performance-based wind engineering paradigm, which decomposes the risk in hazard, vulnerability (or fragility), and exposure.

ERMESS is based on scientific literature models for hazard and vulnerability and industry-provided data for exposure. In fact, it contains a worldwide model for tropical cyclone hazard and a tornado hazard model for the USA. Moreover, it collects more than five-thousand fragility and vulnerability models for buildings and wind-vulnerable components that are categorized based on an ad-hoc taxonomy that aids model selection during the risk analysis. The consequence model is for direct damage to two occupancies.

ERMESS renders these models interoperable in a transparent fashion, for example via embedded procedures for wind intensity conversion, thus enabling their use for a complete risk assessment. Most importantly, it contains a method for component fragility composition, to obtain building fragility. Furthermore, ERMESS can accommodate new models as they become available with the relevant literature, by supporting the addition of user-defined hazard, fragility or vulnerability curves and component damage matrices.

Illustrative examples of the way ERMESS operates were also developed and presented. These examples have shown the feasibility of building fragility composition, using the fragilities of its components, provided that a damage matrix can be defined.

The potential of ERMESS lies in its transparency as a risk assessment tool, transparency that, to the authors' knowledge, is not matched by any similar tool available, and also in its applicability to a large variety of sites and buildings, thus effectively aiding rapid risk assessment for building portfolios in industry applications.

Author's contribution I. I. conceived the study, all authors contributed to the design of the developed tool. Data collection and analysis were performed by all authors, with prevalence of Francesco Pandolfi, who also

coded ERMES. The first draft of the manuscript was written by Francesco Pandolfi under the supervision of the other authors. All authors revised early versions of the manuscript and approved its final version.

Funding Funding for this study was provided by AXA-XL, under the 2019–2021 AXA-XL—DiSt Agreement.

Declarations

Conflict of interest Authors declare they have no financial interests. I. Iervolino and G. Baltzopoulos worked within the 2020–2022 agreement between the University of Naples Federico II and AXA-XL, the P&C and specialty risk division of AXA.

References

- Academy of Disaster Reduction and Emergency Management, Ministry of Emergency Management and Ministry of Education National Disaster Reduction Center of China, Ministry of Emergency Management Information Institute of the Ministry of Emergency Management (2020) 2019 Glob Nat Disaster Assess Rep <https://www.preventionweb.net/publication/2019-global-natural-disaster-assessment-report>
- Amante C, Eakins B (2009) ETOPO1 1 arc-minute global relief model: procedures, data sources and analysis. NOAA Tech Memo NESDIS NGDC-24. <https://doi.org/10.7289/V5C8276M>
- American Society of Civil Engineers (2002) Minimum design loads for buildings and other structures, Standard ASCE 7–02 (SEI of the American Society of Civil Engineers)
- American Society of Civil Engineers (2022) Minimum design loads and associated criteria for buildings and other structures, Standard ASCE 7–22 (SEI of the American Society of Civil Engineers)
- Ascolese S (2022) Analisi di rischio da vento estremo per portafogli di edifici, basata su fragilità di componenti. MSc Thesis in Structural and Geotechnical Engineering, University of Naples Federico II (in Italian)
- Bicheron P, Leroy M, Brockmann C, Krämer U, Miras B, Huc M, Niño F, Defourny P, Vancutsem C, Arino O, Ranera F, Petit D, Amberg V, Berthelot B, Gross D (2006) Globcover: a 300 m global land cover product for 2005 using ENVISAT MERIS time series. Proceeding of the second international symposium on recent advances in quantitative remote sensing, pp 538–542
- Cardona OD, Ordaz MG, Mora MG, Salgado-Gálvez MA, Bernal GA, Zuloaga-Romero D, Cristina M, Yamín L, González D (2014) Global risk assessment: a fully probabilistic seismic and tropical cyclone wind risk assessment. *Int J Disaster Risk Reduct* 10:461–476. <https://doi.org/10.1016/j.ijdr.2014.05.006>
- Ciampoli M, Petrini F, Augusti G (2011) Performance-based wind engineering: towards a general procedure. *Struct Saf* 33(6):367–378. <https://doi.org/10.1016/j.strusafe.2011.07.001>
- CIMNE (2013) Background paper prepared for the global assessment report on disaster risk reduction 2013. Probabilistic Modelling of Natural Risks at the Global Level: Global Risk Model
- Cornell CA, Krawinkler H (2000) Progress and challenges in seismic performance assessment. *PEER Center News* 3:1–3
- Depina I, Divic V, Munjiza A, Peroš B (2021) Performance-based wind engineering assessment of critical telecommunication infrastructure subjected to bora wind. *Eng Struct* 236:112083. <https://doi.org/10.1016/j.engstruct.2021.112083>
- European Committee for Standardization (2005) EN 1991–1–4:2005-Eurocode 1: actions on structures—Part 1–4: general actions—Wind actions
- European Seismological Commission, sub commission on ESWGMS (1998) European Macroseismic Scale 1998 (EMS-98)
- Fan F, Pang W (2019) Tornado hazard analysis and effect of structure size. 13th international conference on applications of statistics and probability in civil engineering (ICASP13). <https://doi.org/10.22725/ICASP13.409>
- Federal Emergency Management Agency (2005) Hazus–MH 2.1-Technical Manual
- Federal Emergency Management Agency (2012) Next-generation methodology for seismic performance assessment of buildings (FEMA P-58)
- Filliben J, Gurley K, Pinelli JP, Simiu E, Subramanian C (2002) Fragility curves, damage matrices, and wind induced loss estimation. *Manag Inf Syst*, 119–126
- Friedman DG (1975) Computer simulation in natural hazard assessment

- Friedman DG (1984) Natural hazard risk assessment for an insurance program. Geneva Pap Risk Insur Issues Pract. <https://doi.org/10.1057/gpp.1984.5>
- Fujita TT (1970) Proposed Characterization of tornadoes and hurricanes by area and intensity. SMRP Research Paper Number 91. <https://swco-ir.tdl.org/handle/10605/261875>
- Gangloff WC (1974) Common mode failure analysis. IEEE PES summer meeting and energy resources conference, 27–30
- Goliger AM, Milford RV (1998) A review of worldwide occurrence of tornadoes. J Wind Eng Ind Aerodyn 74–76:111–121. [https://doi.org/10.1016/S0167-6105\(98\)00009-9](https://doi.org/10.1016/S0167-6105(98)00009-9)
- Griffis L, Patel V, Muthukumar S, Baldava S (2013) A framework for performance-based wind engineering. In: Advances in Hurricane engineering, pp 1205–1216
- Gumaro JJC, Acosta TJS, Tan LRE, Agar JC, Tingatinga EAJ, Musico JKB, Plamenco DAD, Ereño MNC, Pacer JS, Villalba IBO, Hernandez JY Jr (2022) Identification of key components for developing building types for risk assessment against wind loadings: the case of cebu province, philippines. Int J Disaster Risk Reduct 67:102686. <https://doi.org/10.1016/j.ijdrr.2021.102686>
- Hangan H, Kareem A (2021) The oxford handbook of non-synoptic wind storms. Oxford University Press, UK
- Harper BA, Kepert JD, Ginger JD (2010) Guidelines for converting between various wind averaging periods in tropical cyclone conditions. WMO, Geneva
- Hart GC (1976) Estimation of structural damage due to tornadoes. In: symposium on tornadoes: assessment of knowledge and implications for man
- Henderson DJ, Ginger JD (2007) Vulnerability model of an australian high-set house subjected to cyclonic wind loading. Wind Struct 10(3):269–285. <https://doi.org/10.12989/WAS.2007.10.3.269>
- Hendrick R, Friedman D (1966) Potential impacts of storm modification on the insurance industry. Hum Dimens Weather Modif 105:227–248
- Khanduri AC, Morrow GC (2003) Vulnerability of buildings to windstorms and insurance loss estimation. J Wind Eng Ind Aerodyn 91(4):455–467. [https://doi.org/10.1016/S0167-6105\(02\)00408-7](https://doi.org/10.1016/S0167-6105(02)00408-7)
- Knapp KR, Kruk MC, Levinson DH, Diamond HJ, Neumann CJ (2010) The international best track archive for climate stewardship (ibtracs): unifying tropical cyclone data. B Am Meteorol Soc 91:363–376. <https://doi.org/10.1175/2009BAMS2755.1>
- Konthesingha C, Stewart M, Ryan P, Ginger J, Henderson D (2015) Reliability based vulnerability modelling of metal-clad industrial buildings to extreme wind loading for cyclonic regions. J Wind Eng Ind Aerodyn 147:176–185. <https://doi.org/10.1016/j.jweia.2015.10.002>
- Le V, Caracoglia L (2021) Life-cycle cost assessment of vertical structures under nonstationary winds: downburst vs. tornado loads. Eng Struct 243:112515. <https://doi.org/10.1016/j.engstruct.2021.112515>
- Lee KH (2004) Site-specific hazards and load models for probability-based design. Department of Civil, Construction, and Environmental Engineering, Oregon State University, Corvallis, OR
- Lee KH, Rosowsky DV (2005) Fragility assessment for roof sheathing failure in high wind regions. Eng Struct 27(6):857–868. <https://doi.org/10.1016/j.engstruct.2004.12.017>
- Leicester RH, Reardon GF (1976) Statistical Analysis of the structural damage by cyclone Tracy. The Institution of Engineers. https://www.researchgate.net/publication/279581243_A_statistical_analysis_of_the_structural_damage_by_Cyclone_Tracy
- Lin N, Vanmarcke E (2008) Windborne debris risk assessment. Probab Eng Mech 23(4):523–530
- Mason MS, Parackal KI (2017) Vulnerability of buildings and civil infrastructure to tropical cyclones: a preliminary review of modelling approaches and literature. Bushfire Nat Hazards. https://www.bnhrcr.com.au/sites/default/files/managed/downloads/vulnerability_of_buildings_and_civil_infrastructure_to_tropical_cyclones.pdf
- Masoomi H, van de Lindt J (2016) Tornado fragility and risk assessment of an archetype masonry school building. Eng Struct. <https://doi.org/10.1016/j.engstruct.2016.09.030>
- Ouyang Z, Spence SMJ (2019) A performance-based damage estimation framework for the building envelope of wind-excited engineered structures. J Wind Eng Ind Aerodyn 186:139–154. <https://doi.org/10.1016/j.jweia.2019.01.001>
- Ouyang Z, Spence SMJ (2020) A performance-based wind engineering framework for envelope systems of engineered buildings subject to directional wind and rain hazards. J Struct Eng 146(5):4020049. [https://doi.org/10.1061/\(ASCE\)ST.1943-541X.0002568](https://doi.org/10.1061/(ASCE)ST.1943-541X.0002568)
- Ouyang Z, Spence SMJ (2021) Performance-based wind-induced structural and envelope damage assessment of engineered buildings through nonlinear dynamic analysis. J Wind Eng Ind Aerodyn 208:104452. <https://doi.org/10.1016/j.jweia.2020.104452>
- Palutikof JP, Brabson BB, Lister DH, Adcock ST (1999) A review of methods to calculate extreme wind speeds. Meteorol Appl 6(2):119–132. <https://doi.org/10.1017/S1350482799001103>

- Pandolfi F (2022) Performance-based wind risk assessment: computational tools for a building-component oriented vulnerability approach. University of Naples Federico II
- Paulotto C, Ciampoli M, Augusti G (2004) Some proposals for a first step towards a performance based wind engineering. Proceedings of the IFED-international forum in engineering decision making; first forum
- Petruzzelli F (2013) Scale-dependent procedures for seismic risk assessment and management of industrial building portfolios. Università degli Studi di Napoli Federico II
- Petruzzelli F, Iervolino I (2014) FRAME V.1.0: A rapid fragility-based seismic risk assessment tool. In: proceedings of second european conference on earthquake engineering and seismology, 2ECEES, 24–29
- Pinelli J-P, Simiu E, Gurley K, Subramanian C, Zhang L, Cope A, Filliben JJ, Hamid S (2004) Hurricane damage prediction model for residential structures. *J Struct Eng* 130(11):1685–1691. [https://doi.org/10.1061/\(ASCE\)0733-9445\(2004\)130:11\(1685\)](https://doi.org/10.1061/(ASCE)0733-9445(2004)130:11(1685))
- Pita GL (2015) Review of CAPRA Vulnerability Module (Hurricane Suite)
- Preressed Concrete Institute (1971) PCI design handbook: Precast and prestressed concrete
- Qin H, Stewart MG (2019) System fragility analysis of roof cladding and trusses for australian contemporary housing subjected to wind uplift. *Struct Saf* 79:80–93. <https://doi.org/10.1016/j.strusafe.2019.03.005>
- Qin H, Stewart MG (2020) Wind and rain losses for metal-roofed contemporary houses subjected to non-cyclonic windstorms. *Struct Saf* 86:101979. <https://doi.org/10.1016/j.strusafe.2020.101979>
- Sciaudone J, Feuerborn D, Rao G, Daneshvaran S (1997) Development of objective wind damage functions to predict wind damage to low-rise structures. 8th USN
- Solari G (2017) Wind loading of structures: framework, phenomena, tools and codification. *Structures*. <https://doi.org/10.1016/j.istruc.2017.09.008>
- Sparks PR, Schiff SD, Reinhold TA (1994) Wind damage to envelopes of houses and consequent insurance losses. *J Wind Eng Ind Aerodyn* 53(1–2):145–155. [https://doi.org/10.1016/0167-6105\(94\)90023-X](https://doi.org/10.1016/0167-6105(94)90023-X)
- Standard Association of Australia (2002) Structural design actions—part 2: wind actions. *As/nzs 1170(2):2002*
- Standohar-Alfano CD, van de Lindt JW (2015) Empirically based probabilistic tornado hazard analysis of the United States using 1973–2011 data. *Nat Hazards Rev* 16(1):04014013. [https://doi.org/10.1061/\(ASCE\)NH.1527-6996.0000138](https://doi.org/10.1061/(ASCE)NH.1527-6996.0000138)
- Tan C, Fang W (2018) Mapping the wind hazard of global tropical cyclones with parametric wind field models by considering the effects of local factors. *Int J Disaster Risk Sci* 9(1):86–99. <https://doi.org/10.1007/s13753-018-0161-1>
- The MathWorks Inc (2020) MATLAB-Release R2020 Update 4 9.8.0. 1417392. The MathWorks Inc
- Tokyo Polytechnic University (2007) Aerodynamic database of non-isolated low-rise buildings. http://www.wind.arch.tkougai.ac.jp/info_center/windpressure/grouplowrise/mainpage.html
- Unanwa CO, McDonald JR, Mehta KC, Smith DA (2000) The development of wind damage bands for buildings. *J Wind Eng Ind Aerodyn* 84(1):119–149. [https://doi.org/10.1016/S0167-6105\(99\)00047-1](https://doi.org/10.1016/S0167-6105(99)00047-1)
- UNISDR (2013) Global Assessment Report on Disaster Risk Reduction. <https://www.undrr.org/publication/global-assessment-report-disaster-risk-reduction-2013>
- van de Lindt JW, Dao TN (2009) Performance-based wind engineering for wood-frame buildings. *J Struct Eng* 135(2):169–177. [https://doi.org/10.1061/\(ASCE\)0733-9445\(2009\)135:2\(169\)](https://doi.org/10.1061/(ASCE)0733-9445(2009)135:2(169))
- Vickery PJ, Lin J, Skerlj PF, Twisdale L, Huang K (2006a) HAZUS-MH hurricane model methodology. I: hurricane hazard, terrain, and wind load modeling. *Nat Hazard Rev* 7:82–93
- Vickery PJ, Skerlj PF (2005) Hurricane gust factors revisited. *J Struct Eng* 131(5):825–832. [https://doi.org/10.1061/\(ASCE\)0733-9445\(2005\)131:5\(825\)](https://doi.org/10.1061/(ASCE)0733-9445(2005)131:5(825))
- Vickery PJ, Skerlj PF, Lin J, Twisdale L, Young MA, Lavelle F (2006b) HAZUS-MH hurricane model methodology. II: damage and loss estimation. *Nat Hazard Rev* 7:94–103
- Ward PJ, Blauhut V, Bloemendaal N, Daniell JE, de Ruiter MC, Duncan MJ, Emberson R, Jenkins SF, Kirschbaum D, Kunz M, Mohr S, Muis S, Riddell GA, Schäfer A, Stanley T, Veldkamp TIE, Winsemius HC (2020) Review article: natural hazard risk assessments at the global scale. *Nat Hazard Earth Sys Sci* 20:1069–1096. <https://doi.org/10.5194/nhess-20-1069-2020>
- Wehner M, Ginger J, Holmes J, Sandland C, Edwards M (2010) Development of methods for assessing the vulnerability of australian residential building stock to severe wind. *IOP Conf Ser Earth Environ Sci*. <https://doi.org/10.1088/1755-1315/11/1/012017>
- Wind science and engineering center (2004) A Recommendation for an Enhanced Fujita scale (EF-Scale)
- World Meteorological Organization (WMO) (2021) Review for the forty years of WMO tropical cyclone programme (1980–2020) In: *Natural Hazards and Earth System Sciences Vol 1270*

- Yamin LE, Hurtado AI, Barbat AH, Cardona OD (2014) Seismic and wind vulnerability assessment for the GAR-13 global risk assessment. *Int J Disaster Risk Reduct* 10:452–460. <https://doi.org/10.1016/j.ijdrr.2014.05.007>
- Zhang S, Nishijima K, Maruyama T (2014) Reliability-based modeling of typhoon induced wind vulnerability for residential buildings in Japan. *J Wind Eng Ind Aerodyn* 124:68–81. <https://doi.org/10.1016/j.jweia.2013.11.004>

Publisher's Note Springer Nature remains neutral with regard to jurisdictional claims in published maps and institutional affiliations.

Springer Nature or its licensor (e.g. a society or other partner) holds exclusive rights to this article under a publishing agreement with the author(s) or other rightsholder(s); author self-archiving of the accepted manuscript version of this article is solely governed by the terms of such publishing agreement and applicable law.